Physics and Astronomy Faculty Publications

Physics and Astronomy

7-2011

The Role of Hole Localization in Sacrificial Hydrogen Production by Semiconductor-Metal Heterostructured Nanocrystals

Krishna P. Acharya

Rony S. Khnayzer

Timothy O'Connor

Geoffrey Diederich

Maria Kirsanova

See next page for additional authors

Follow this and additional works at: https://scholarworks.bgsu.edu/physics_astronomy_pub

Part of the Astrophysics and Astronomy Commons, and the Physics Commons

Author(s)

Krishna P. Acharya, Rony S. Khnayzer, Timothy O'Connor, Geoffrey Diederich, Maria Kirsanova, Anna
Klinkova, Daniel Roth, Erich Kinder, Martene Imboden, and Mikhail Zamkov

The Role of Hole Localization in Sacrificial Hydrogen Production by Semiconductor−Metal Heterostructured Nanocrystals

Krishna P. Acharya,[†,§] Rony S. Khnayzer,[†,‡] Timothy O'Connor,[§] Geoffrey Diederich,[§] Maria Kirsanova,[†,§] Anna Klinkova,[†,§] Daniel Roth,[§] Erich Kinder,[§] Martene Imboden,[‡] and Mikhail Zamkov*,[†,§]

[†]The Center for Photochemical Sciences, [‡]Department of Chemistry, and [§]Department of Physics, Bowling Green State University, Bowling Green, Ohio 43403, United States

Ⓢ Supporting Information

ABSTRACT: The effect of hole localization on photocatalytic activity of Pt-tipped semiconductor nanocrystals is investigated. By tuning the energy balance at the semiconductor−ligand interface, we demonstrate that hydrogen production on Pt sites is efficient only when electron-donating molecules are used for stabilizing semiconductor surfaces. These surfactants play an important role in enabling an efficient and stable reduction of water by heterostructured nanocrystals as they fill vacancies in the valence band of the semiconductor domain, preventing its degradation. In particular, we show that the energy of oxidizing holes can be efficiently transferred to a ligand moiety, leaving the semiconductor domain intact. This allows reusing the inorganic portion of the "degraded" nanocrystal-ligand system simply by recharging these nanoparticles with fresh ligands.

KEYWORDS: Photovoltaics, photocatalysis, quantum dots, nanorods

The increasing demand for renewable energy sources requires a significant effort to be invested in the development of inexpensive and efficient light-harvesting materials.[1] Of particular interest is the photocatalytic production of solar hydrogen from water, which allows converting sunlight directly into usable fuels, thus avoiding potential problems associated with energy storage. Photocatalytic hydrogen production is also favored thermodynamically, as most of the solar power is delivered at photon energies that are capable of driving the water splitting reaction ($\lambda < 1100$ nm). Our ability to harvest these resources comes down to a number of technological challenges that are largely synthetic in nature. Among those, the design of materials that efficiently absorb solar radiation and convert the photon energy into long-lived charge-separated states is of key importance.

Over the past decade, the field of photocatalysis has witnessed a spur of activity, aided by the significant advances in nanotechnology and nanofabrication of semiconductor and metal nanostructures, which resulted in the development of several successful strategies for extending the spectral range of photocatalysts beyond that of ultraviolet-primed TiO_2. Doping,[2−5] metal ion implantation,[6−10] modification of oxide surfaces with molecular or nanocrystal sensitizers,[11−17] employment of alternative materials based on novel metal oxides[18−20] and sulfide[21−27] semiconductors, and semiconductor composites[28−34] have all been considered for driving catalysis in the visible and near-IR portions of the solar spectrum. In particular, sulfide semiconductor-based photocatalysts have been witnessing an increased amount of attention in past years, motivated, in part, by excellent light-harvesting characteristics of material such as ZnS, and CdS. It is

expected that for the production of solar hydrogen to be commercially viable in the next decade,[18] the quantum efficiency of water splitting reactions should be at least 30% at 600 nm or near 75% at the CdS absorption edge ($\lambda \approx 460$ nm), which is a realistic target in light of the fact that the best photocatalysts based on nanostructured CdS show yields nearly on the par with this target value.[35−37] Despite these advances, the task of fabricating sulfide semiconductor composites that can simultaneously exhibit efficient absorption, charge separation, and red/ox steps still poses tremendous challenges associated with such technical issues as "backward" charge recombination, side reactions, and material photocorrosion.

One potentially rewarding strategy deployable for the production of solar fuels has been recently presented through the advances in the synthesis of CdS-based metal−semiconductor (M-S) nanocrystals (NCs).[38,39] These nanoparticles are formed via coupling of several crystalline domains, each with its unique functionality into a composite nano-object that can drive an efficient separation of photoinduced charges, therefore precluding premature electron−hole recombination. Impressive photocatalytic activity of visible-range semiconductor/metal composites utilizing CdSe/Au,[40] CdS/Pt,[35,41,42] CdS-PdX,[43] and CdSe/CdS/Pt[44] material systems has been observed in several recent experiments through water splitting and the reduction of organic dyes. The relative success of these methods was attributed to the two key factors of the composite architecture: the visible-range absorbance of CdS and CdSe
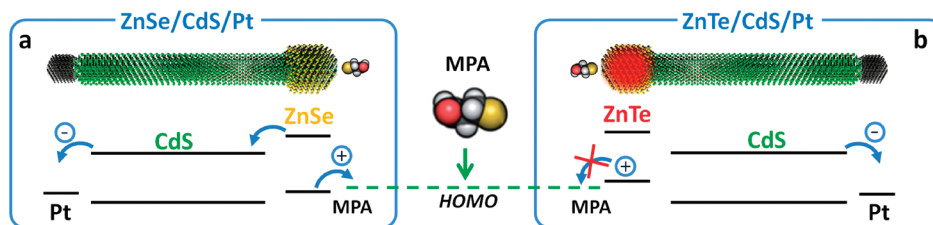
Figure 1. Electronic level diagram showing a relative alignment of excited state energies in ZnSe/CdS/Pt (a) and ZnTe/CdS/Pt (b) hetero-nanocrystals. Quantitative information on these energy levels for both systems is provided in Figure SF1 (Supporting Information). Upon excitation, an electron−hole pair is efficiently separated at heterointerfaces of the two semiconductor materials with electrons residing in the CdS and holes in the ZnSe(Te) domain of the structure. Subsequently, photoinduced holes undergo further localization, the character of which is determined by the relative alignment of hole energies at the semiconductor−ligand interface. For instance, in the case of ZnSe-terminated nanorods, the photoinduced hole is accepted by the ligand molecule (MPA, MUA) and expelled to the surface of the composite nanoparticle; while for ZnTe-terminated nanorods, the hole is confined inside the semiconductor domain.

semiconductors and the existence of epitaxial bonds at the M-S domain interfaces, which promote fast injection of carriers into the metal catalyst.[45] Moreover, the use of heterostructured CdSe/CdS nanointerfaces has been demonstrated to further increase the quantum yield of hydrogen production through the spatial separation of charges in nonadjacent CdSe and Pt domains of CdSe/CdS/Pt heteronanocrystals.[44]

At the present stage, the potential benefits of CdS-based photocatalysts associated with high efficiencies in the visible range and spatially extended separation of charges are compromised by the limited stability of these materials in comparison with their oxide counterparts. Indeed, sulfides are subject to rapid photocorrosion by oxidizing holes, which convert some of the excitation energy into chemical decomposition of the semiconductor into sulfur and metal ions.[19,20] The stability issue becomes even more important in light of the fact that for photocatalysts to be commercially viable, the cost of the produced H_2 should exceed the cost of platinum utilized as a catalytic domain of the structure, which puts a constraint on the minimum number of water splitting cycles that a single nanoparticle should perform before its irreversible degradation ($>10^6-10^9$).[46] The use of sacrificial agents can facilitate the process of hole removal suppressing the photocorrosion; however, in order to be efficiently scavenged, the hole first needs to be promoted to the surface of the semiconductor domain. This issue is of central importance to nanoscale photocatalysts comprising heterostructured interfaces (e.g., CdSe/CdTe,[47,48] CdSe/CdS,[49] or ZnSe/CdS[50,51]). These heteronanocrystals efficiently separate electron−hole pairs, preventing their "backward" recombination, but tend to trap holes in one of the NC domains, causing its decomposition as well as the degradation of the S/M interface.[44] Consequently, the main challenge concerning the development of sulfide-based semiconductor photocatalysts is no longer associated with maximizing quantum efficiencies, which for systems such as CdS/Pt and CdSe/CdS/Pt already reach 80−90%,[42] but is shifted toward the more pressing issue of regenerating photoinduced holes that impede the production of H_2 via several mechanisms, including decomposition of the semiconductor, photocorrosion of the M/S interface, and the slowdown of the photocatalytic turnover cycle.

Here, we investigate the effect of hole localization on the sacrificial hydrogen production by ZnSe/CdS/Pt and ZnTe/CdS/Pt heterostructured nanorods composed of one metal (M) and two semiconductor (S_1, S_2) domains (see Figure 1). The three components of the composite nanostructure are chosen to

form a linear energy gradient, which drives photoinduced carriers to localize in nonadjacent parts of the nanorod, with holes residing in the S_1 and electrons in the M domains. The resulting spatially extended localization of carriers helps suppress the "backward" recombination of charges, leading to efficient harvesting of visible photons through the injection of electrons into the Pt catalytic site.

Tuning the localization of photoinduced holes in fabricated heteronanocrystals was achieved by varying the energy level of the S_1 semiconductor material with respect to the HOMO level of the surface ligand. As shown in Figure 1, when ZnSe material is incorporated as the S_1 component of the nanorod, photogenerated holes are driven to the surface of the structure due to exothermic electron transfer from the HOMO level of the hydrophilic ligand (mercaptopropionic acid (MPA) or mercaptoundecanoic acid (MUA)) to the valence band of the ZnSe material. Meanwhile, when ZnTe semiconductor, for which the valence band energy lies above the ligand HOMO level, is employed in lieu of ZnSe, photoinduced holes remain trapped in the S_1 domain giving rise to a different mechanism of carrier decay. The two investigated nanorod morphologies, therefore, represent the two opposing cases of the hole localization pattern, corresponding to the surface (ZnSe/CdS/Pt) and volumetric (ZnTe/CdS/Pt) confinement of positive charges.

The comparison of photocatalytic activity in ZnSe/CdS/Pt and ZnTe/CdS/Pt heteronanocrystals revealed that hydrogen production on the Pt site is efficient only when electron-donating molecules are used as surface ligands. These surfactants appear to be of key importance in enabling an efficient and stable reduction of water by CdS-based heteronanocrystals as they fill the vacancy in the valence band of the semiconductor domain, preventing its degradation. In particular, it is demonstrated that volumetric confinement of the photoinduced hole within the S_1 semiconductor domain (ZnTe/CdS/Pt) leads to a 300-fold suppression of H_2 production rate on Pt when compared to a ZnSe/CdS/Pt system, for which holes are expelled to the surface of the structure and scavenged by methanol. The present experiments also demonstrate that the degree of charge separation in heterostructured heteronanocrystals (e.g., CdSe/CdS, ZnSe/CdS, ZnTe/CdS) does not significantly contribute to the rate of H_2 production since the transfer of photoinduced holes to the surface of the structure occurs at a substantially faster rate ($\tau < 1$ ns) than "backwards" carrier recombination ($\tau \approx 30-50$ ns). Nevertheless, the use of photocatalytic heteronanocrystals that separate photoinduced charges across heterostructured interfaces may be
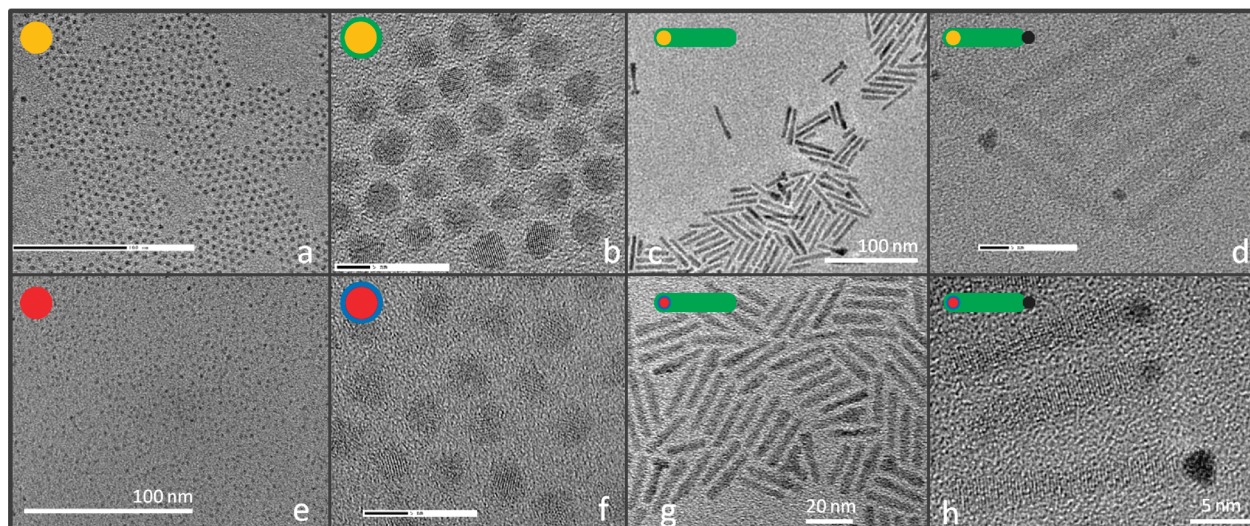
Figure 2. Transmission electron microscopy (TEM) images of ZnSe/CdS/Pt and ZnTe/CdS/Pt heteronanocrystals corresponding to the four consecutive stages of the growth protocol: (a) ZnSe seed NCs; (b) ZnSe NCs with a few monolayers of the CdS shell; (c) ZnSe/CdS nanorods grown from ZnSe/CdS core/shell NCs; (d) ZnSe/CdS nanorods after Pt deposition; (e) ZnTe NCs; (f) ZnTe/CdSe core/shell NCs; (g) ZnTe/CdSe/CdS nanorods grown from ZnTe/CdSe seeds; (h) ZnTe/(CdSe)/CdS nanorods after Pt deposition.

important for shielding the S/M boundary from oxidation by the photoinduced hole.

Perhaps the most interesting outcome of the present study was the demonstration that semiconductor heteronanocrystals utilizing electron-donating ligands degrade primarily via ligand desorption, with minimal decomposition of the inorganic lattice. In particular, we show that the energy of oxidizing holes can be efficiently transferred to a ligand moiety, leaving the semiconductor domain intact. This allows for recharging of "degraded" nanoparticles with fresh ligands, thus extending the life span of expensive inorganic materials (Pt), a task which cannot be easily achieved using homogeneous metallo-organic photocatalysts that tend to degrade irreversibly.[52]

Synthesis of ZnSe/CdS/Pt colloidal heteronanocrystals was performed according to previously reported protocols[50,51,53] using a four-step procedure. Typically, small-diameter ZnSe NCs were prepared using hot-injection methods, overcoated with a thin shell of CdS (approximately three monolayers), and used to seed the growth of CdS nanorods, onto which Pt tips were deposited. The length of CdS nanorods was controlled by varying the amount of ZnSe seeds in the reaction flask.[51] To fabricate ZnTe/CdS/Pt nanostructures, ZnTe seeds were first capped with a few monolayers (ML) of the CdSe shell, serving as a stress-relief layer at the interface of ZnTe and CdS materials (ZnTe/CdS strain = 4.5%, and ZnTe/CdSe = 0.4%[54]). The presence of CdSe shell has also helped in passivating the surface of air-sensitive ZnTe, resulting in the enhancement of the band gap emission in ZnTe/CdSe core/shell NCs, as compared to that of bare ZnTe cores. Following the synthesis of ZnTe/CdSe seeds, the subsequent growth of CdS nanorod extensions and Pt tips proceeded according to the aforementioned protocol used for the growth of ZnSe/CdS/Pt heterostructures. Detailed procedures for the synthesis of ZnSe/CdS/Pt and ZnTe/CdS/Pt heteronanocrystals are provided in the Supporting Information.

Figure 2 shows several characteristic transmission electron microscopy (TEM) images of fabricated heteronanocrystals corresponding to the four consecutive stages of the growth

protocol. ZnSe and ZnTe NC seeds, fabricated in the first step of the procedure (Figure 2a,e), exhibited a low dispersion of nanoparticles sizes (6.8% for ZnSe, 8.4% for ZnTe) and were approximately round in shape, which gave rise to the formation of uniform ZnSe/CdS and ZnTe/CdSe core/shell composites in the second stage (panels b and f of Figure 2, respectively, and Figure SF2 (Supporting Information)). For both structures, the shell was evenly distributed on the surface of core NCs, as was expected due to a relatively small strain at respective heteromaterial interfaces (2.7% for ZnSe/CdS and 0.4% for ZnTe/CdSe). The subsequent growth of CdS extensions onto nanoparticle seeds was confirmed through the observation of characteristic nanorod-shaped specimens (Figure 2c,g) with an average aspect ratio of 6.2. The average length of grown nanorods was estimated to be 25.5 nm, with a standard length dispersion of 11%. Lastly, the deposition of Pt onto CdS nanorods of both nanomaterial systems resulted in the growth of ≈3 nm metal tips (Figure 2d,h), forming primarily on one side of heteronanocrystals. Such anisotropic growth of Pt was first demonstrated by Mokari et al.[53] and was attributed to the wurtzite crystalline structure of CdS nanorods promoting uneven rates of Pt nucleation on Cd- and S-rich nanorod facets.

The character of carrier localization in fabricated heteronanocrystals capped with hydrophobic ligands was substantiated based on their respective optical properties. For ZnSe NCs, the growth of CdS shell was accompanied by the onset of the emission at $\lambda = 490$ nm (Figure 3b), resulting from the "spatially indirect" recombination of carriers, $1S(e)_{CdS} \rightarrow 1S_{3/2}(h)_{ZnSe}$, a process which is commonly observed in type II semiconductor heteronanocrystals.[55−57] As was previously demonstrated by ultrafast spectroscopy studies,[51,58,59] the existence of epitaxial associations at ZnSe/CdS nanostructured interfaces promotes a fast separation of photoinduced charges with electrons localizing in the CdS domain and holes in the ZnSe domain of the composite nanoparticle. The resulting charge separated state subsequently decays through a spatially indirect radiative recombination, distinguishable in the FL spectra as a red-shifted emission peak (Figure 3b). The radiative lifetime corresponding
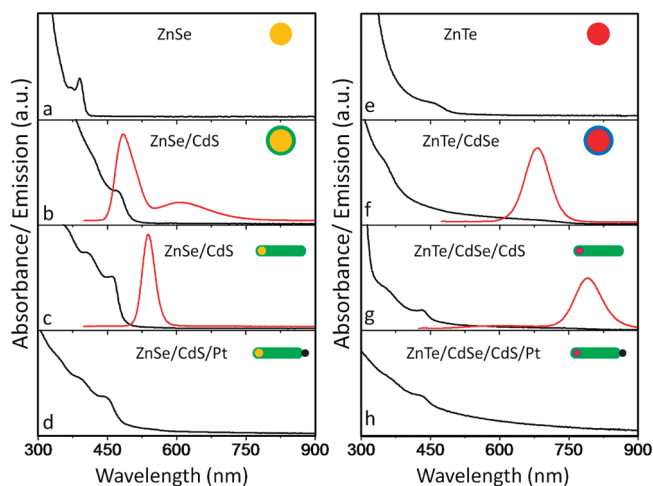
Figure 3. Optical properties of fabricated heteronanocrystals. (a) The absorbance of ZnSe NCs showing an excitonic feature at $\lambda = 390$ nm. Band-edge emission was not observed for these samples. (b) ZnSe NCs overcoated with a 1 nm thick shell of CdS, for which the onset of quasi-type II[39] carrier confinement regime is evidenced through red-shifted absorption ($\lambda \approx 475$ nm) and emission peaks ($\lambda \approx 490$ nm). (c) Emission and absorbance of ZnSe/CdS nanorods grown from ZnSe/CdS core/shell NCs. (d) Absorbance of ZnSe/CdS nanorods after Pt deposition. (e−h) Emission and absorbance spectra associated with the four-step synthesis of ZnTe/CdS/CdS/Pt heteronanocrystals: (e) ZnTe NCs, (f) ZnTe/CdSe core/shell NCs, (g) ZnTe/CdSe/CdS nanorods grown from ZnTe/CdSe seeds, (h) ZnTe/(CdSe)/CdS nanorods after Pt deposition.

to this transition is typically longer than that of binary semiconductor NCs,[50] as expected due to a relatively small spatial overlap of carrier wave functions in type II systems.[60] Upon growth of CdS extensions, the emission feature at $\lambda = 470$ nm further red shifts to $\lambda = 535$ nm (Figure 3c), reflecting the delocalization-induced decrease in the energy of $1S_{CdS}$ electrons, associated with the nanorod morphology.[51,61] Notably, the photon energy corresponding to this emission band is below the band gap energy of either ZnSe or CdS NCs, which further confirms that the recombination of carriers occurs via spatially indirect transitions. Upon deposition of Pt tips, the emission of heteronanocrystals was quenched due to a combined effect of photoinduced charge transfer of electrons into M domains and trapping of carriers at the CdS/Pt interface.[45] The residual FL signal observed in nanoparticle samples after Pt deposition is believed to arise from those structures for which the Pt tip is either missing or too small to suppress radiative decay of CdS excitons. Growth of Pt tips has also resulted in the modification of the absorbance profile of ZnSe/CdS nanorods, distinguishable as an apparent widening of CdS excitonic features. This phenomenon was previously observed in Au/CdS composites and was attributed to the delocalization of the S electronic states into M domains.[45]

Similar to ZnSe/CdS heteronanocrystals, the band edge alignment in ZnTe/CdS nanorods promotes spatial separation of photoinduced charges across the ZnTe/(CdSe)/CdS interface with electrons residing in CdS and holes in ZnTe domains of the structure. The formation of charge-separated excitons is manifested through the red-shifted emission of $1S(e)_{CdSe} \rightarrow 1S(h)_{ZnTe}$ (Figure 3f) and $1S(e)_{CdS} \rightarrow 1S(h)_{ZnTe}$ (Figure 3g) interfacial states with associated photon energies that fall below
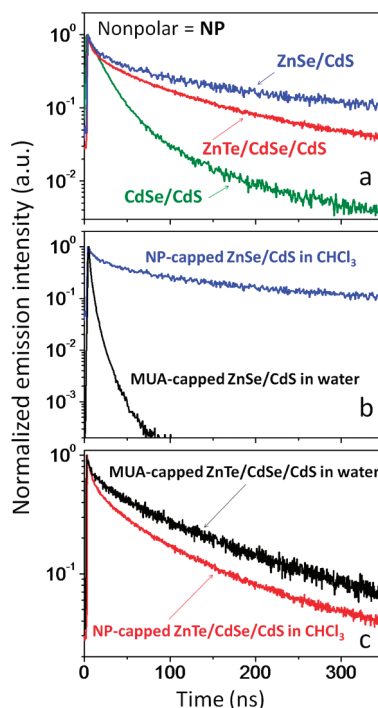

Figure 4. Summary of fluorescence lifetime measurements. (a) Comparison of the FL intensity decay traces observed for ZnSe/CdS (blue), ZnTe/CdSe/CdS (red), and CdSe/CdS (green) composite nanorods capped with nonpolar (NP) ligands. Longer lifetimes correspond to a smaller spatial overlap between electron and hole wave functions in these structures. (b) Comparison of the FL lifetime of ZnSe/CdS nanorods capped with nonpolar (blue) and MUA ligands (black). The dramatic decrease in the exciton lifetime upon OA (HDA, TOP) → MUA ligand exchange is attributed to the transfer of photoinduced holes to MUA molecules. (c) FL lifetime of ZnTe/CdSe/CdS nanorods capped with NP (red) and MUA ligands (black).

the band gap of either material. The spatial separation of charges in ZnTe/(CdSe)/CdS heteronanocrystals is also confirmed by the observation of increased radiative lifetimes ($\tau = 59$ ns, Figure 4) of $1S(e)_{CdS} - 1S(h)_{ZnTe}$ excitons, which reflects the reduction in the spatial overlap of electron and hole wave functions. Similar to ZnSe/CdS heterostructures, the growth of Pt tips on ZnTe/CdS nanorods resulted in quenching of the emission.

In addition to interfacial morphology, another important factor affecting carrier localization in fabricated heteronanocrystals is the energetics of surface ligands, which are arguably just as critical to the ensuing decay dynamics as the interdomain alignment of electronic levels. Typically, surfaces of CdS nanostructures fabricated via hot-injection synthesis are capped with a combination of oleic acid (OA), tri-n-octylphosphine (TOP), and hexadecylamine (HDA) hydrophobic ligands, all of which provide a significant potential barrier to electrical charges in these nanostructures. As a result, charge carrier wave functions in as-prepared nanorods are confined inside the nanostructure with relatively low amplitudes on nanoparticle surfaces. The localization pattern of carriers in these structures, however, can undergo significant changes when hydrophobic ligands are replaced with hydrophilic MPA or MUA molecules. These ligands lower the potential barrier for photoinduced holes in the valence band (see Figure 1), giving rise to the delocalization of charges or a transfer

of holes to a ligand moiety. As was demonstrated by previous works, HOMO levels of MPA hydrophilic ligands are higher in energy than those of valence holes in a number of semiconductor NCs including CdSe(S) and ZnSe(S) NCs,[62] which explains the significant suppression of the FL emission in these materials following the OA → MPA ligand exchange.[63] On the other hand, when the valence band of the semiconductor NC is located above the MPA HOMO level, the hole remains confined within the NC domain enabling the emission of NC−MPA complexes. The mechanism of the hole transfer in the semiconductor−ligand system has been well exemplified in the case of CdTe NCs whose valence band lies 0.3 eV above that of MPA,[62,64] resulting an increased emission of these colloids upon OA → MPA ligand exchange.[65]

The effect of surface ligands on electronic properties of investigated heterostructures can be readily predicted from known energies of valence holes in ZnSe and ZnTe NCs and their relative positions with respect to the HOMO level of MPA and MUA hydrophilic ligands. According to the energy diagram in Figure 1, MPA ligands are expected to scavenge holes from ZnSe, but not ZnTe core NCs, potentially leading to observable differences in the emission of ZnSe and ZnTe-seeded CdS NRs. This hypothesis is confirmed by the FL measurements of MUA-capped heteronanocrystals, revealing that the emission of ZnSe/CdS NRs was completely quenched upon OA → MUA ligand exchange, while the emission of ZnTe/CdSe/CdS nanostructures remained similar in intensity (Figure SF3, Supporting Information). The fact that the emission yield of ZnTe-seeded NR was virtually unaffected by the OA → MUA ligand exchange suggests that quenching of the emission in ZnSe/CdS heteronanocrystals was not the result of nanoparticle aggregation or charge trapping on CdS surfaces, since both ZnSe- and ZnTe-based heteronanocrystals were prepared in the same manner and, therefore, undergone copious surface treatment. Furthermore, both nanoparticle types produced clear aqueous solutions that were stable for weeks in an ambient environment (especially when longer-chain MUA molecules were used for stabilization), indicating that surfaces of these heteronanocrystals were adequately passivated. Therefore, the observed quenching of FL in MPA- or MUA-capped ZnSe/CdS heterostructures was attributed to the energetically favorable transfer of photoinduced holes to surface ligands.

FL lifetime measurements provide further evidence that the transfer of photoinduced holes is the dominant process contributing into quenching of emission in MUA-capped ZnSe/CdS heterostructures. Indeed, according to Figure 4a, the exciton lifetime in ZnSe/CdS ($\lambda = 540$ nm) is reduced from 42.0 to 1.9 ns upon ligand exchange, indicating a fast depletion of charges in these nanoparticles, meanwhile, the FL lifetime of ZnTe-seeded NRs increases from 31 to 59 ns when OA ligands are replaced with MUA. Notably, the near-exponential shape of the FL decay trace in ZnSe/CdS NCs is consistent with a charge-transfer-induced quenching of emission, since processes associated with poor passivation and carrier trapping usually contribute a non-exponential tail into the decay curve which may extend into a microsecond range. On the basis of these observations, we conclude that MUA ligands efficiently remove photoinduced holes from ZnSe NCs while preventing the NC-to-ligand charge transfer in ZnTe-seeded NRs. The upper limit, associated with the hole transfer time in ZnSe-MPU systems, was estimated to be 1.9 ns, although, the actual transfer time could be substantially shorter than this value, since the FL intensity decay method often
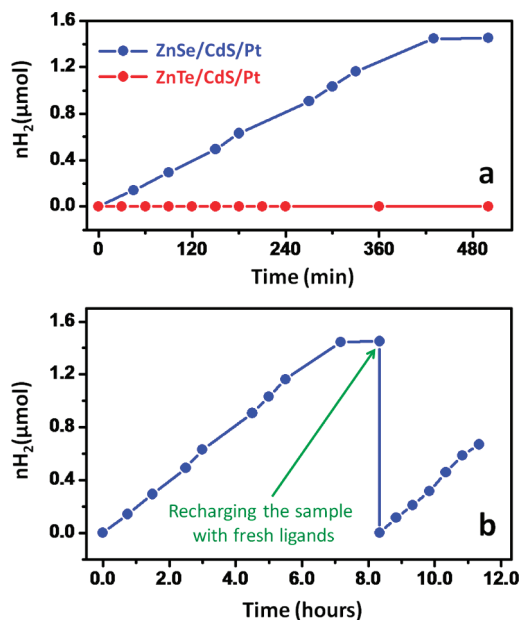

Figure 5. (a) Evolution of hydrogen production on ZnSe/CdS/Pt (blue) and ZnTe/CdS/Pt (red) heteronanocrystals capped with MUA ligands. The substantial difference in the amount of generated hydrogen between the two materials is attributed to the dynamics of photoinduced holes in the semiconductor−ligand system. (b) The hydrogen production is resumed upon recharging ZnSe/CdS/Pt nanoparticles with fresh MUA ligands. The H_2 production rate (the slope of the experimental curve) after addition of fresh ligands (8−12 h) is approximately the same as that prior to the initial degradation (0−8 h).

underestimates the charge transfer rates in coupled NC systems.[66]

To understand the role of hole localization on the rate of hydrogen production, we compare the efficiency of water splitting reaction by ZnTe/CdS/Pt and ZnSe/CdS/Pt heteronanocrystal systems, corresponding to hole-confining and hole-delocalizing regimes, respectively. For H_2 production experiments, both heteronanocrystals were capped with either MPA or MUA ligands, dispersed in water/methanol (8:1 by volume) mixture, and subsequently degassed in a sealed cuvette with argon bubbling for 30 min. The reaction samples, containing approximately 1 mg of nanocrystals in 5 mL of liquid, were then illuminated using the filtered output of a 300 W arc xenon lamp (Oriel) through a fiber optic (Oriel) providing approximately 120 mW/cm^2 of spectrally integrated emission. The hydrogen gas was detected from the headspace and analyzed in a gas chromatograph (Shimadzu GC-8A, argon carrier gas) equipped with a 5 Å molecular sieve column (Restek) and thermal conductivity detector. The number of H_2 moles was estimated from a calibration curve.

Figure 5a shows the integrated amount of produced H_2 versus irradiation time for ZnTe/CdS/Pt and ZnSe/CdS/Pt heteronanocrystals. In the first seven hours of the reaction, the rate of H_2 generation on ZnSe/CdS/Pt nanoparticles is several orders of magnitude greater than that of ZnTe/CdS/Pt, indicating that the water splitting process is far more efficient on heteronanocrystals, which expel the photoinduced hole to the surface. We note that surfaces of both heteronanocrystals are morphologically the same, such that the observed difference in the H_2 production rates can be attributed solely to the energetics of the seed
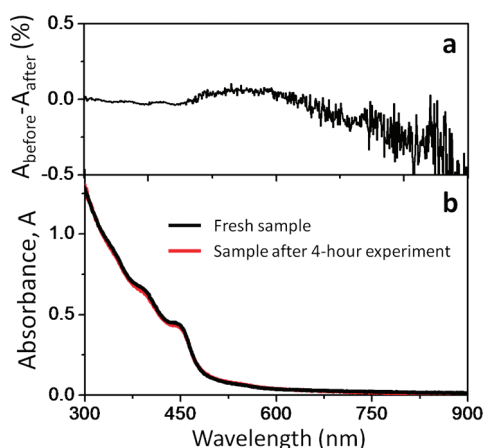
Figure 6. Analysis of sample degradation. The absorbance of fresh (black) and degraded ZnSe/CdS/Pt (red) samples is compared in (b) and the associated difference is plotted in (a). The data indicate that the degradation of the inorganic lattice during water splitting is minimal. This is consistent with the fact that the energy of the oxidizing hole is transferred to ligands, which eventually desorb, ceasing the hydrogen production.

nanoparticle (ZnSe, ZnTe). To provide further experimental support to this hypothesis, CdSe seeds, which are expected to donate holes to MUA ligands, were used in lieu of ZnSe in H_2 production tests. According to Figure SF5 (Supporting Information), the rate of H_2 generation by CdSe/CdS/Pt heteronanocrystals was found to be nearly the same as in the case of ZnSe/CdS/Pt composites. These results highlight the important role of surface ligands in hydrogen production by sulfide-based semiconductor nanoparticles. We expect that properly chosen ligands with corresponding HOMO energies designed to drive the photoinduced hole transfer from the semiconductor domain can be used to achieve additional improvements in the efficiency of H_2 production by sulfide semiconductor—metal composites.

The life span of ZnSe/CdS/Pt photocatalysts observed under 120 mW/cm^2 illumination in H_2 production experiments averaged 5—7 h (see Figure 4), which is within the typical range of degradation times observed for homogeneous photocatalytic systems based on metallo-organic compositions.[52,67—69] The degradation of the latter has been the subject of many investigations and is attributed to the decomposition of some or all components of the photocatalytic assembly often accompanied by the decolorization of the solution.[52] Conversely, the degradation mechanism associated with the present material system is not well-known and is of a particular interest in view of the fact that oxidizing holes, deemed to cause the corrosion of sulfide semiconductors, are now driven away from the CdS/Pt interface and subsequently expelled to the surface of the structure.

To explain the mechanism of ZnSe/CdS/Pt degradation during the water splitting reaction, we have compared *normalized* absorbance profiles of "degraded" and freshly prepared heteronanocrystals (Figure 6). According to Figure 6a, the shape of the ZnSe/CdS/Pt absorption after several hours of the water splitting reaction was nearly unchanged, with maximum differences in the profile of degraded and fresh nanoparticles not exceeding 0.1% across the visible range. The observation of such small changes suggests that structural decomposition of ZnSe/CdS/Pt nanorods was negligible and, therefore, unlikely to be the main cause for the observed suppression of H_2 production. While the morphology of

ZnSe/CdS/Pt heteronanocrystals did not change as a result of the photocatalytic reaction, the solubility of these nanoparticles in aqueous solutions has decreased significantly. In contrast to fresh samples that were stable in water for several days, the "degraded" heteronanocrystals precipitated within hours of the reaction, indicating possible formation of nanoparticle aggregates. This result was also consistent with Fourier transform infrared spectroscopy (FTIR) measurements of degraded samples, showing a noticeable decrease in the amount of MUA ligand on heteronanocrystal surfaces (see Figure SF6, Supporting Information). On the basis of these observations, we propose that the suppression of H_2 production on ZnSe/CdS/Pt observed in the present experiments was caused primarily by the desorption of surface ligands and not the structural degradation of the semiconductor lattice.

The observed desorption of surface ligands, responsible for the loss of photocatalytic activity in ZnSe/CdS/Pt heteronanocrystals, can be attributed to their key role in removing photoinduced holes from the semiconductor, which exposes these molecules to oxidation. Notably, upon addition of fresh MUA molecules to "degraded" ZnSe/CdS/Pt nanorods, the production of H_2 was resumed at nearly 100% of the original rate (see Figure 5b). *These experiments highlight an important fact: the inorganic domain of the nanorod—ligand system can be reused even after the production of H_2 has stopped, simply by recharging the samples with fresh surface ligands.* It should be noted that the demonstrated recovery of photocatalytic properties upon recharging of MUA was tested only for the case of charge-separating heteronanocrystals that efficiently expel holes via surface ligands, whereas systems such as CdS/Pt may experience some decomposition of the S-M interface. Additional research into the dynamics of charge carriers in sulfide semiconductor—ligand photocatalysts will help answer these important questions.

In conclusion, the effect of hole localization on the photocatalytic activity of CdS-based heterostructured heteronanocrystals was investigated. The two nanoparticle morphologies, comprising Pt-tipped dot-in-a-rod ZnSe/CdS and ZnTe/CdS structures designed to efficiently separate photoinduced charges were used to simulate two different regimes of sacrificial water reduction, corresponding to the localization of holes inside (ZnTe/CdS/Pt) and on the surface (ZnSe/CdS/Pt) of the composite nanoparticle. It was found that the rate of H_2 production was substantially greater for ZnSe/CdS/Pt heteronanocrystals that efficiently expel photoinduced holes to the surface of the structure via ZnSe-to-ligand charge transfer. The ability of surface ligands to accept oxidizing holes was also found to be crucial in preventing the degradation of the semiconductor—metal composites. In particular it was found that the energy carried by the hole was efficiently absorbed by the ligand/scavenger system leaving the structural integrity of the ZnSe/CdS/Pt nanoparticles intact. These findings highlight the importance of choosing proper energetics of the ligand—semiconductor system for improving both the efficiency and the stability of homogeneous photocatalytic water reduction in the presence of sacrificial agents. In particular, we expect that the use of rechargeable, electron-donating ligands may significantly improve the turnover numbers of photocatalytic composites utilizing charge-separating semiconductor heterointerfaces.

■ ASSOCIATED CONTENT

ⓢ Supporting Information. Details of synthesis, X-ray power diffraction data (XRD), and additional emission and FTIR

spectra. This material is available free of charge via the Internet at http://pubs.acs.org.

■ AUTHOR INFORMATION

Corresponding Author
*E-mail: zamkovm@bgsu.edu.

■ ACKNOWLEDGMENT

■ REFERENCES

(1) Lewis, N. S.; Nocera, D. G. *Proc. Natl. Acad. Sci. U.S.A.* **2006**, *103*, 15729–15735.

(2) Li, H. X.; Bian, Z. F.; Zhu, J.; Huo, Y.; Li, H.; Lu, Y. *J. Am. Chem. Soc.* **2007**, *129*, 4538–4539.

(3) Huo, Y.; Bian, Z.; Zhang, X.; Jin, Y.; Zhu, J.; Li, H. *J. Phys. Chem. C* **2008**, *112*, 6546–6550.

(4) Rengifo-Herrera, J. A.; Mielczarski, E.; Mielczarski, J.; Castillo, N. C.; Kiwi, J.; Pulgarin, C. *Appl. Catal., B* **2008**, *84*, 448–456.

(5) Wu, P. G.; Xie, R. C.; Shang, J. K. *J. Am. Ceram. Soc.* **2008**, *91*, 2957–2962.

(6) Takeuchi, M.; Yamashita, H.; Matsuoka, M.; Anpo, M.; Hirao, T.; Itoh, N.; Iwamoto, N. *Catal. Lett.* **2000**, *67*, 135–137.

(7) Yamashita, H.; Harada, M.; Misaka., J.; Takeuchi, M.; Ichihashi, Y.; Goto, F.; Ishida, M.; Sasaki, T.; Anpo, M. *J. Synchrotron Radiat.* **2001**, *8*, 569–571.

(8) Yamashita, H.; Harada, M.; Misaka, J.; Takeuchi, M; Ikeue, K.; Anpo, M. *J. Photochem. Photobiol., A* **2002**, *148*, 257–261.

(9) Anpo, M.; Takeuchi, M. *J. Catal.* **2003**, *216*, 505–516.

(10) Yamashita, H.; Harada, M.; Misaka, J.; Takeuchi, M.; Neppolian, B.; Anpo, M. *Catal. Today* **2003**, *84*, 191–196.

(11) Gurunathan, K.; Maruthamuthu, P.; Sastri, V. C. *Int. J. Hydrogen Energy* **1997**, *22*, 57–62.

(12) Dhanalakshmi, K. B.; Latha, S.; Anandan, S.; Maruthamuthu, P. *Int. J. Hydrogen Energy* **2001**, *26*, 669–674.

(13) Jin, J.; Zhang, X.; Lu, G.; Li, S. *J. Mol. Catal. A: Chem.* **2006**, *259*, 275–280.

(14) Jin, Z. L.; Zhang, X. J.; Li, Y. X.; Li, S. B.; Lu, G. X. *Catal. Commun.* **2007**, *8*, 1267–1273.

(15) Hussein, F. H.; Alkhateeb, A. N. *Desalination* **2007**, *209*, 350–355.

(16) Yao, K. S.; Cheng, T. C.; Li, S. J.; Yang, L. Y.; Tzeng, K. C.; Chang, C. Y.; Ko, Y. *Surf. Coat. Technol.* **2008**, *203*, 922–924.

(17) Harris, C.; Kamat, P. V. *ACS Nano* **2009**, *3*, 682–690.

(18) Maeda, K.; Domen, K. *J. Phys. Chem. C* **2007**, *111*, 7851–7861.

(19) Osterloh, F. E. *Chem. Mater.* **2008**, *20*, 35–54.

(20) Kudo, A.; Miseki, Y. *Chem. Soc. Rev.* **2009**, *38*, 253–278.

(21) Kudo, A. *Int. J. Hydrogen Energy* **2006**, *31*, 197–202.

(22) Tsuji, I.; Kato, H.; Kudo, A. *Angew. Chem., Int. Ed.* **2005**, *44*, 3565–3568.

(23) Reber, J. F.; Rusek, M. *J. Phys. Chem.* **1986**, *90*, 824–834.

(24) Shangguan, W.; Yoshida, A. *J. Phys. Chem. B* **2002**, *106*, 12227–12230.

(25) Lei, Z.; Ma, G.; Liu, M.; You, W.; Yan, H.; Wu, G.; Takata, T.; Hara, M.; Domen, K.; Li, C. *J. Catal.* **2006**, *237*, 322–329.

(26) Tsuji, I.; Kato, H.; Kudo, A. *Chem. Mater.* **2006**, *18*, 1969–1975.

(27) Khon, E; Hewa-Kasakarage, N. N.; Nemitz, I; Acharya, K.; Zamkov, M. *Chem. Mater.* **2010**, *22*, 5929–5936.

(28) Kang, M. G.; Han, H. E.; Kim, K. J. *J. Photochem. Photobiol., A* **1999**, *125*, 119–125.

(29) So, W. W.; Kim, K. J.; Moon, S. J. *Int. J. Hydrogen Energy* **2004**, *29*, 229–234.

(30) De, G. C; Roy, A. M.; Bhattacharya, S. S. *Int. J. Hydrogen Energy* **1996**, *21*, 19–23.

(31) Keller, V.; Garin, F. *Catal. Commun.* **2003**, *4*, 377–383.

(32) Nguyen, T. V.; Kim, S. S.; Yang, O. B. *Catal. Commun.* **2004**, *5*, 59–62.

(33) Tennakone, K.; Bandara, J. *Appl. Catal., A* **2001**, *208*, 335–341.

(34) Li, D.; Haneda, H.; Ohashi, N; Hishita, S.; Yoshikawa, Y. *Catal. Today* **2004**, *93–95*, 895–901.

(35) Bao, N.; Shen, L.; Takata, T.; Domen, K. *Chem. Mater.* **2008**, *20*, 110–117.

(36) Navarro, R. M.; Sanchez-Sanchez, M. C.; Alvarez-Galvan, M. C.; del Valle, F.; Fierro, J. L. G. *Energy Environ. Sci.* **2009**, *2*, 35–54.

(37) Hernandez-Alonso, M. D.; Fresno, F.; Suareza, S.; Coronado, J. M. *Energy Environ. Sci.* **2009**, *2*, 1231–1257.

(38) Carbone, L.; Cozzoli, P. D. *Nano Today* **2010**, *5*, 449–493.

(39) Donegá, C. M. *Chem. Soc. Rev.* **2011**, *40*, 1512–1546.

(40) Costi, R.; Saunders, A. E.; Elmalem, E.; Salant, A.; Banin, U. *Nano Lett.* **2008**, *8*, 637–641.

(41) Elmalem, E.; Saunders, A. E.; Costi, R.; Salant, A.; Banin, U. *Adv. Mater.* **2008**, *20*, 4312–4317.

(42) Berr, M.; Vaneski, A.; Susha, A. S.; Rodríguez-Fernández, J.; Döblinger, M.; Jäckel, F.; Rogach, A. L.; Feldmann, J. *Appl. Phys. Lett.* **2010**, *97*, 093108.

(43) Shemesh, Y; Macdonald, J; Menagen, G; Banin, U. *Angew. Chem., Int. Ed.* **2011**, *50*, 1185–1189.

(44) Amirav, L.; Alivisatos, P. A. *J. Phys. Chem. Lett.* **2010**, *1*, 1051–1054.

(45) Khon, E.; Mereshchenko, A.; Tarnovsky, A. N.; Acharya, K.; Klinkova, A.; Hewa-Kasakarage, N. N.; Nemitz, I.; Zamkov, M. *Nano Lett.* **2011**, *11*, 1792–1799.

(46) Mallouk, T. E. *J. Phys. Chem. Lett.* **2010**, *1*, 2738–2739.

(47) Halpert, J. E.; Porter, V. J.; Zimmer, J. P.; Bawendi, M. G. *J. Am. Chem. Soc.* **2006**, *128*, 12590.

(48) Donegá, C. M. *Phys. Rev. B* **2010**, *81*, 165303.

(49) Carbone, L.; Nobile, C.; de Giorgi, M.; Sala, F. D.; Morello, G.; Pompa, P.; Hytch, M.; Snoeck, E.; Fiore, A.; Franchini, I. R.; Nadasan, M.; Silvestre, A. F.; Chiodo, L.; Kudera, S.; Cingolani, R.; Krahne, R.; Manna, L. *Nano Lett.* **2007**, *7*, 2942–2950.

(50) Dorfs, D.; Salant, A.; Popov, I; Banin, U. *Small* **2008**, *4*, 1319–1323.

(51) Hewa-Kasakarage, N. N.; Kirsanova, M.; Nemchinov, A.; Schmall, N.; El-Khoury, P. Z.; Tarnovsky, A. N.; Zamkov, M. *J. Am. Chem. Soc.* **2009**, *131*, 1328–1334.

(52) Wang, X.; Goeb, S.; Ji, Z.; Pogulaichenko, N. A.; Castellano, F. N. *Inorg. Chem.* **2011**, *50*, 705–707.

(53) Habas, S. E.; Yang, P.; Mokari, T. *J. Am. Chem. Soc.* **2008**, *130*, 3294–3295.

(54) Singh, J. *Physics of Semiconductors and Their Heterostructures*; McGraw-Hill: New York, 1993.

(55) Nemchinov, A.; Kirsanova, M.; Hewa-Kasakarage, N. N.; Zamkov, M. *J. Phys. Chem. C* **2008**, *112*, 9301–9307.

(56) Ivanov, S. A.; Piryatinski, A.; Nanda, J.; Tretiak, S.; Zavadil, K. R.; Wallace, W. O.; Werder, D.; Klimov, V. I. *J. Am. Chem. Soc.* **2007**, *129*, 11708–11719.

(57) Kirsanova, M.; Nemchinov, A.; Hewa-Kasakarage, N. N.; Schmall, N.; Zamkov *Chem. Mater.* **2009**, *21*, 4305–4309.

(58) Hewa-Kasakarage, N. N.; El-Khoury, P. Z.; Tarnovsky, A. N.; Kirsanova, M.; Nemitz, I.; Nemchinov, A.; Zamkov, M. *ACS Nano* **2010**, *4*, 1837–1844.

(59) Hewa-Kasakarage, N. N.; El-Khoury, P. Z.; Schmall, N.; Kirsanova, M.; Nemchinov, A.; Tarnovsky, A. N.; Bezryadin, A.; Zamkov, M. *Appl. Phys. Lett.* **2009**, *94*, 133113–133115.

(60) Chuang, C. H.; Lo, S. S.; Scholes, G. D.; Burda, C. *J. Phys. Chem. Lett.* **2010**, *1*, 2530–2535.

(61) Steiner, D.; Dorfs, D.; Banin, U.; Sala, F. D.; Manna, L.; Millo, O. *Nano Lett.* **2008**, *8*, 2954–2958.

(62) Völker, J.; Zhou, X.; Ma, X.; Flessau, S.; Lin, H.; Schmittel, M.; Mews, A. *Angew. Chem., Int. Ed.* **2010**, *49*, 6865–6868.

(63) Talapin, D. V.; Rogach, A. L.; Kornowski, A.; Haase, M.; Weller, H. *Nano Lett.* **2001**, *1*, 207–211.

(64) Wuister, S. F.; Donega, C. D.; Meijerink, A. *J. Phys. Chem. B* **2004**, *108*, 17393–17397.

(65) Alivisatos, A. P.; Gu, W. W.; Larabell, C. *Annu. Rev. Biomed. Eng.* **2005**, *7*, 55–76.

(66) Pijpers, J. J. H.; Koole, R.; Evers, W. H.; Houtepen, A. J.; Boehme, S.; De Mello Donegá, C.; Vanmaekelbergh, D.; Bonn, M. *J. Phys. Chem. C* **2010**, *114*, 18866–18873.

(67) Cline, E. D.; Adamson, S. E.; Bernhard, S. *Inorg. Chem.* **2008**, *47*, 10378–10388.

(68) Yamauchi, K.; Masaoka, S.; Sakai, K. *J. Am. Chem. Soc.* **2009**, *131*, 8404–8406.

(69) Fihri, A.; Artero, V.; Razavet, M.; Baffert, C.; Leibl, W.; Fontecave, M. *Angew. Chem., Int. Ed.* **2008**, *47*, 564–567.